doi:10.1093/brain/awz370 BRAIN 2020: 143; 131–149 | 131

BRAIN
A JOURNAL OF NEUROLOGY

The coding and non-coding transcriptional landscape of subependymal giant cell astrocytomas

Anika Bongaarts,[1] Jackelien van Scheppingen,[1] Anatoly Korotkov,[1] Caroline Mijnsbergen,[1] Jasper J. Anink,[1] Floor E. Jansen,[2] Wim G.M. Spliet,[3] Wilfred F.A. den Dunnen,[4] Victoria E. Gruber,[5] Theresa Scholl,[5] Sharon Samueli,[5] Johannes A. Hainfellner,[6] Martha Feucht,[5] Katarzyna Kotulska,[7] Sergiusz Jozwiak,[7,8] Wieslawa Grajkowska,[9] Anna Maria Buccoliero,[10] Chiara Caporalini,[10] Flavio Giordano,[11] Lorenzo Genitori,[11] Roland Coras,[12] Ingmar Blümcke,[12] Pavel Krsek,[13] Josef Zamecnik,[14] Lisethe Meijer,[15] Brendon P. Scicluna,[16] Antoinette Y.N. Schouten-van Meeteren,[15,17] Angelika Mühlebner,[1,*] James D. Mills[1,*] and Eleonora Aronica[1,18,*]

[*]These authors contributed equally to this work.

Tuberous sclerosis complex (TSC) is an autosomal dominantly inherited neurocutaneous disorder caused by inactivating mutations in *TSC1* or *TSC2*, key regulators of the mechanistic target of rapamycin complex 1 (mTORC1) pathway. In the CNS, TSC is characterized by cortical tubers, subependymal nodules and subependymal giant cell astrocytomas (SEGAs). SEGAs may lead to impaired circulation of CSF resulting in hydrocephalus and raised intracranial pressure in patients with TSC. Currently, surgical resection and mTORC1 inhibitors are the recommended treatment options for patients with SEGA. In the present study, high-throughput RNA-sequencing (SEGAs n = 19, periventricular control n = 8) was used in combination with computational approaches to unravel the complexity of SEGA development. We identified 9400 mRNAs and 94 microRNAs differentially expressed in SEGAs compared to control tissue. The SEGA transcriptome profile was enriched for the mitogen-activated protein kinase (MAPK) pathway, a major regulator of cell proliferation and survival. Analysis at the protein level confirmed that extracellular signal-regulated kinase (ERK) is activated in SEGAs. Subsequently, the inhibition of ERK independently of mTORC1 blockade decreased efficiently the proliferation of primary patient-derived SEGA cultures. Furthermore, we found that LAMTOR1, LAMTOR2, LAMTOR3, LAMTOR4 and LAMTOR5 were overexpressed at both gene and protein levels in SEGA compared to control tissue. Taken together LAMTOR1–5 can form a complex, known as the 'Ragulator' complex, which is known to activate both mTORC1 and MAPK/ERK pathways. Overall, this study shows that the MAPK/ERK pathway could be used as a target for treatment independent of, or in combination with mTORC1 inhibitors for TSC patients. Moreover, our study provides initial evidence of a possible link between the constitutive activated mTORC1 pathway and a secondary driver pathway of tumour growth.

1 Department of (Neuro)Pathology, Amsterdam UMC, University of Amsterdam, Amsterdam, The Netherlands
2 Department of Pediatric Neurology, University Medical Center Utrecht, Utrecht, The Netherlands
3 Department of Pathology, University Medical Center Utrecht, Utrecht, The Netherlands
4 Department of Pathology and Medical Biology, University of Groningen, University Medical Center Groningen, Groningen, The Netherlands
5 Department of Pediatrics, Medical University of Vienna, Vienna, Austria
6 Institute of Neurology, Medical University of Vienna, Vienna, Austria

Received April 1, 2019. Revised September 13, 2019. Accepted October 1, 2019. Advance Access publication December 13, 2019

7 Department of Neurology and Epileptology, Children's Memorial Health Institute, Warsaw, Poland
8 Department of Child Neurology, Medical University of Warsaw, Warsaw, Poland
9 Department of Pathology, Children's Memorial Health Institute, Warsaw, Poland
10 Pathology Unit, Anna Meyer Children's Hospital, Florence, Italy
11 Department of Neurosurgery, Anna Meyer Children's Hospital, Florence, Italy
12 Department of Neuropathology, University Hospital Erlangen, Erlangen, Germany
13 Department of Paediatric Neurology, Charles University, 2nd Faculty of Medicine, Motol University Hospital, Prague, Czech Republic
14 Department of Pathology and Molecular Medicine, Charles University, 2nd Faculty of Medicine, Motol University Hospital, Prague, Czech Republic
15 Princess Máxima Center for Pediatric Oncology, Utrecht, The Netherlands
16 Center for Experimental and Molecular Medicine and Department of Clinical Epidemiology, Biostatistics and Bioinformatics, Amsterdam UMC, University of Amsterdam, Amsterdam, The Netherlands
17 Department of Pediatric Oncology, Emma Children's Hospital, Amsterdam UMC, University of Amsterdam, Amsterdam, The Netherlands
18 Stichting Epilepsie Instellingen Nederland (SEIN), The Netherlands

Correspondence to: Dr James D. Mills
Department of Neuropathology, Amsterdam UMC, Location AMC, Meibergdreef 9, 1105 AZ
Amsterdam, The Netherlands
E-mail: j.d.mills@amc.uva.nl

Correspondence may also be addressed to: Dr Angelika Mühlebner
E-mail: a.muehlebnerfahrngruber@amc.nl

Keywords: SEGA; TSC; sequencing; low grade glioma

Abbreviations: DEGs = differentially expressed genes; MAPK = mitogen-activated protein kinase; mTORC1 = mechanistic target of rapamycin complex 1; RNA-Seq = RNA sequencing; RT-qPCR = real-time quantitative PCR; SEGAs = subependymal giant cell astrocytomas; TSC = tuberous sclerosis complex

Introduction

Tuberous sclerosis complex (TSC) is a multisystem genetic disorder affecting approximately 1 million individuals worldwide. It is caused by mutations in either *TSC1* or *TSC2* and is characterized by the development of benign tumours in multiple organs, including the brain (European Chromosome 16 Tuberous Sclerosis Consortium, 1993; van Slegtenhorst *et al.*, 1997; DiMario, 2004). In the CNS, TSC is associated with subcortical/cortical tubers, subependymal nodules and subependymal giant cell astrocytomas (SEGAs) (Mizuguchi and Takashima, 2001; Aronica *et al.*, 2012; Aronica and Crino, 2014).

SEGAs are benign slow growing tumours classified as WHO grade I representing 1–2% of all paediatric brain tumours and occur almost exclusively in patients with TSC (Jozwiak *et al.*, 2015; Louis *et al.*, 2016). The prevalence of SEGAs in patients with TSC ranges from 5% to 25% and they usually arise during the first two decades of life (Cuccia *et al.*, 2003; Goh *et al.*, 2004; Adriaensen *et al.*, 2009; Kothare *et al.*, 2014; Kingswood *et al.*, 2017). SEGAs arise around the ventricle zone, mostly at the height of the foramen of Monro and are thought to develop from subependymal nodules (Morimoto and Mogami, 1986; Fujiwara *et al.*, 1989; Nabbout *et al.*, 1999). Despite their slow growing nature, extended growth of the tumour can cause obstruction of the cerebral fluid tract leading to (acute) hydrocephalus and in rare cases even sudden death (de Ribaupierre *et al.*, 2007; Kotulska *et al.*, 2014).

Hamartin (*TSC1*), tuberin (*TSC2*) and TBC1 domain family member 7 (TBC1D7) can form a complex containing a GTPase-activating protein (GAP) for the small GTPase Ras homologue enriched in brain 1 (RHEB1), a direct positive regulator of the mechanistic target of rapamycin complex 1 (mTORC1) located on the late endosome/lysosome surface (Inoki *et al.*, 2003; Sancak *et al.*, 2008; Dibble *et al.*, 2012). Loss of function mutations in *TSC1* or *TSC2* result in constitutive activation of the mTORC1 pathway (CHan *et al.*, 2004). In TSC, germline mutations in *TSC1* or *TSC2* can be familial inherited in a autosomal dominant fashion, but more often are sporadic in nature. Furthermore, loss of heterozygosity of *TSC1* or *TSC2* has been reported in ~80% of SEGAs (CHan *et al.*, 2004; Bongaarts *et al.*, 2017; Martin *et al.*, 2017). However, 'second-hit' mutations in *TSC1* and *TSC2* are not always observed in brain lesions including SEGA, suggesting that additional genetic events are involved in the growth and progression of SEGAs. Several studies have reported an activation of the mitogen-activated protein kinase (MAPK)/extracellular signal-regulated kinase (ERK) pathway in SEGA (Han *et al.*, 2004; Ma *et al.*, 2005, 2007) and it has been shown that inhibiting ERK can effect the proliferation of SEGA cells (Tyburczy *et al.*, 2010), indicating that the MAPK/ERK pathway could play an important role in SEGA development. Furthermore, it has been shown

that both the mTORC1 and MAPK/ERK pathway can be activated by the lysosomal Ragulator complex consisting of late endosomal/lysosomal adaptor, MAPK and mTOR activator 1–5 (LAMTOR1/p18, LAMTOR2/p14, LAMTOR3/MP1, LAMTOR4/C7orf59 and LAMTOR5/HBXIP) (Teis *et al.*, 2002; Bar-Peled *et al.*, 2012; Nada *et al.*, 2014; de Araujo *et al.*, 2017). Therefore, the role of the Ragulator complex in the development of SEGAs warrants further investigation.

Current treatment options for growing SEGAs include surgical resection or use of mTORC1 inhibitors, such as everolimus and rapamycin (Franz *et al.*, 2006, 2013, 2014, 2015; Krueger *et al.*, 2010; Kotulska *et al.*, 2013; Krueger *et al.*, 2013). Although mTORC1 inhibitors have been shown to be effective in patients with TSC, the response to mTORC1 inhibitors can be variable and cessation of treatment may result in tumour regrowth (Franz *et al.*, 2006, 2014; Bissler *et al.*, 2008; Krueger *et al.*, 2010, 2016; McCormack *et al.*, 2011; Martins *et al.*, 2013).

Previous gene expression studies on SEGA focus on the expression of protein-coding genes using either a microarray (Tyburczy *et al.*, 2010) or RNA sequencing (RNA-seq; Martin *et al.*, 2017). In the present study, we aimed to map both the protein-coding and non-coding RNA, including small RNAs, of SEGA compared to periventricular control tissue in order to identify signaling pathways deregulated in SEGA and explore the possibility of novel therapeutic targets.

Materials and methods

SEGA tumour specimens

Twenty-one SEGA specimens were obtained from the following sites: Amsterdam UMC (location AMC), University Medical Center Utrecht, University Medical Center Groningen, Medical University of Vienna, Children's Memorial Health Institute in Warsaw and Meyer Children's Hospital in Florence. Nineteen of the 21 SEGA samples included in this study were obtained from patients who met the clinical diagnostic criteria for TSC. From the 21 SEGA samples 19 were selected and used for RNA-sequencing (RNA-Seq) (Table 1). When DNA material permitted, *TSC1*/*TSC2* mutation analysis was performed as part of routine clinical care on blood or tumour sample DNA or was determined using massively parallel sequencing (including analysis of loss of heterozygosity) as described previously (Northrup *et al.*, 2013; Bongaarts *et al.*, 2017) (Table 1). Histological diagnosis was confirmed following the current WHO classification guidelines by two independent neuropathologists (Louis *et al.*, 2016). The following clinical data were extracted from medical records: *TSC1*/*TSC2* mutation status, gender, localization of the resected area, age at seizure onset, duration of active epilepsy, drug management at time of surgery (including treatment with mTORC1 inhibitors), size of the tumour, tumour recurrence/regrowth and presence of other TSC-related malformations. No peri-tumoural tissue was available, therefore periventricular brain tissue was obtained (as well as one sample of cortex tissue) from autopsy controls without a history of TSC, epilepsy or brain tumours. Thirteen controls were obtained of which eight were selected for RNA-Seq and five were used for additional immunohistochemistry. Additionally, four cortical tubers, one angiomyolipoma and one sample of normal renal tissue were obtained from TSC patients who met the clinical diagnostic criteria for TSC (Supplementary Table 1). Specimens were obtained and used in accordance with the Declaration of Helsinki and this study was approved by the Medical Ethics Committees of each institution.

RNA isolation and RNA sequencing

For RNA isolation frozen tissue or cultured cells were homogenized with Qiazol Lysis Reagent (Qiagen). The total RNA including the microRNA (miRNA) fraction was isolated using the miRNeasy Mini kit (Qiagen) according to manufacturer's instructions. The concentration of RNA was determined using a NanoDrop™ 2000 spectrophotometer (Thermo Fisher Scientific) for cell cultures or Qubit® 2.0 Fluorometer (Life Technologies) for frozen tissue. For RNA-Seq the RNA integrity was assessed using a Bioanalyser 2100 (Agilent). Library preparation and sequencing were completed at GenomeScan. The Illumina RNA-Seq and TruSeq Small RNA-Seq sample preparation kits were used to prepare sequencing libraries of mRNA and small RNA in accordance to manufacturers guidelines. Clustering and DNA sequencing was performed using the Illumina cBot and HiSeq 2500 according to manufacturer's protocols. Each library was subjected to paired-end sequencing, producing reads of 125 nucleotides in length with a read-depth of 36 million reads for RNA-Seq and 12 million reads for small RNA-Seq.

Bioinformatics analysis of RNA-Sequencing data

Read quality was assessed using FastQC v0.11.5 (Babraham Institute, Babraham, Cambridgeshire, UK). Trimmomatic v0.36 was used to trim and filter reads of low quality (Bolger *et al.*, 2014). Low quality leading and trailing bases were removed from each read, the quality of the body of the reads was assessed with a sliding window trimming using a window of 4 and a Phred score threshold of 20 and 15 nucleotides, in our RNA and small RNA datasets, respectively. Reads that dropped below 80 nucleotides in our RNA dataset and 17 nucleotides, in our small RNA datasets, as well as reads with no partner forward or reverse read were excluded from further analysis.

For small RNA-Seq paired-end reads were aligned to the reference genome, GRCh38 using TopHat2 v2.0.13 (Kim *et al.*, 2013). No mismatches were allowed between the trimmed reads and the reference genome and small RNA reads were allowed to align a maximum of 10 times (Kim *et al.*, 2013). Next, transcripts for each sample were assembled *de novo* using Cufflinks v2.2.1 using the default settings, except that the expression of each transcript was not corrected for length (Trapnell *et al.*, 2012). The transcript assembly for each sample, along with a custom reference annotation consisting of short RNA species extracted from Gencode v25

Table 1 Summary of clinicopathological features of patients with SEGA

SEGA #	Age, years	Gender	Mutation	Tumour location	Epilepsy	Age of onset	Frequency	Tumour recurrence/ regrowth	Tumour size, mm	AED[a]	mTOR inhibitors	Other clinical manifestations
1[b,d]	10	Male	*TSC2*	Ventricle	Yes	3 years	5–10 per day	No	42	Yes	No	Unknown
2[b]	11	Female	*TSC2*	Ventricle	No	None	None	No	Unknown	No	No	No other signs for TSC
3[b]	8	Male	*TSC2*	Ventricle	Yes	4 months	None	No	31	Yes	No	Cortical tuber, AML
4[b,c,d]	13	Female	*TSC1*	Ventricle	Yes	17 months	Monthly	No	40	Yes	No	Cortical tuber
5[b,e]	1	Male	*TSC2*	Ventricle	Yes	1 month	Daily	No	30	Yes	Yes (non-responder)	Multiple SEGAs, cortical tubers, drug resistant epilepsy
6[b]	13	Male	*TSC2*	Left caudate nucleus	Yes	6 months	Weekly	No	20	Yes	Yes (responder)	Tubers, minor psycho-motor delay, SEN
7[b]	14	Male	*TSC2*	Foramen of Monro	No	None	None	No	5	No	No	Renal cysts
8[b,c,b]	4	Male	*TSC1*	Ventricle	Yes	3 months	> 10 per month	Yes	5	Yes	No	Cortical tuber
9[b]	7	Female	*TSC2*	Ventricle	Yes	5 months	> 10 per day	No	45	Yes	No	Unknown
10[b,c,d]	17	Female	*TSC2*	Ventricle	No	None	None	No	27	No	No	No other signs for TSC
11[b]	1	Female	*TSC2*	Ventricle	Yes	1 month	Daily	No	30	Yes	No	Cortical tuber
12[b]	13	Male	*TSC2*	Ventricle	Yes	4 months	1 per week	Yes	20	Yes	No	Cortical tuber
13[b]	24	Male	*TSC1*	Ventricle	Yes	6 years	5–10 per day	No	40	Yes	No	Unknown
14[b]	8	Male	NMI	Left caudate nucleus	Yes	1 year	Weekly	No	30	Yes	No	Minor psychomotor delay
15[b]	9	Male	*TSC1*	Right caudate nucleus	Yes	2 years	Monthly	No	30	Yes	No	None
16[b]	28	Female	Unknown	Unknown	Yes	Unknown	Unknown	Unknown	Unknown	No	No	Cortical tuber
17[b]	33	Male	Unknown	Basal nuclei	Yes	6 months	Daily	Yes	30	Yes	No	Cortical tubers, autism, drug resistant epilepsy, behaviour problems (aggressivity)
18[b]	1	Male	Unknown	Left caudate nucleus	Yes	8 months	Monthly	No	20	Yes	No	Minor psychomotor delay, cortical tubers
19[b,c]	28	Male	*TSC2*	Ventricle	Yes	7 years	3 per day	Yes	34	Yes	No	Unknown
20 [c,d]	16	Male	*TSC1*	Ventricle	No	None	None	No	42	No	No	Cortical tubers, mild angiofibroma
21[c,d,e]	1	Male	*TSC2*	Ventricle	Yes	1 month	Daily	No	30	Yes	No	Multiple SEGAs, cortical tubers, drug resistant epilepsy

[a]The most commonly used AEDs were carbamazepin, vigabatrin, valproate and topiramate; however, each patient had a personalized drug treatment regime.
SEGA samples used for [b]RNA-Seq and RT-qPCR, [c]western blotting or [d]immunohistochemistry.
[e]SEGA samples obtained from same patient.
AED = antiepileptic drugs; AML = angiomyolipoma; SEN = subependymal nodule.

(Harrow *et al.*, 2012) and miRNAs from miRBase21 (Griffiths-Jones *et al.*, 2008) were passed onto Cuffmerge v2.2.1 (Trapnell *et al.*, 2012). Cuffmerge compared the *de novo* transcript assembly of each sample with reference annotation of known miRNAs and short non-coding RNAs. This allowed each assembled transcript to be classified as a known short non-coding species, miRNAs or as a novel short non-coding RNA. Next, all assembled novel transcripts >100 nucleotides were removed from the analysis. Subsequently, the chromosomal location of the novel short non-coding RNAs were compared to the location of the known genes, based on GENCODE v25, and were classified as unannotated intergenic or unannotated gene derived. These elements were then all merged together to create a final reference annotation that consisted of miRNAs, short RNA species, unannotated intergenic short RNA or unannotated gene derived short RNAs. This reference annotation file along with the original small RNA read alignment files were passed to featureCounts from the Subread package and the number of reads that aligned to each transcripts were counted (Liao *et al.*, 2014).

For the RNA dataset paired-end reads were aligned to the reference genome, GRCh38 using TopHat2 v2.0.13 and the default settings (Kim *et al.*, 2013). The number of reads that aligned to each gene, based on GENCODE v25, were determined using the featureCounts program from the Subread package (Liao *et al.*, 2014). The RNA and small RNA count matrices were passed on to the R package DESeq2 and were normalized using the median of ratios method ((Love *et al.*, 2014). Genes and small RNAs with a Benjamini-Hochberg adjusted *P*-value < 0.05 were considered differentially expressed. The biotypes of all the differentially expressed genes (DEGs) were assessed using BioMart (Smedley *et al.*, 2009). Based on the biotype assigned by BioMart the genes were further grouped into five categories: (i) protein-coding: all genes with protein-coding ability; (ii) pseudogenes: all genes classified as one of the following; polymorphic pseudogene, processed pseudogene, unprocessed pseudogene, or transcribed processed pseudogene; (iii) long non-coding RNAs: all genes classed as long non-coding RNAs; (iv) undefined: genes which could not be classified; and (v) other: genes that had one or more biotypes or did not fit into any of the aforementioned categories.

Target prediction tools

RNA-Seq and small RNA-Seq data were integrated using the R package 'piano' (Varemo *et al.*, 2013) and custom scripts written in R. The 'piano' package is an open-source tool for performing gene set enrichment analysis (GSEA) using a selection of available methods. The whole RNA transcriptome profile and the Reactome (Croft *et al.*, 2011; Fabregat *et al.*, 2018) gene to pathway dataset were passed to 'piano'. The Wilcoxon rank-sum test method was used to identify enriched gene sets amongst the dataset. Significance values were calculated through random gene sampling. Briefly, a random set of genes equal in size to the gene set being tested was selected and the gene set statistic was recalculated (Varemo *et al.*, 2013). This was repeated 10 000 times to give a discrete null distribution. The gene set *P*-value was based on the fraction of random gene set statistics that are equal to or more extreme than the original gene set statistic. All *P*-values were corrected using the Benjamini-Hochberg method. Gene sets with an adjusted *P*-value < 0.05 for non-directional, mixed-directional up and mixed-directional down were considered enriched. Next, gene sets that were enriched for DEGs were identified using Fisher's exact test. Gene sets with a Benjamini-Hochberg adjusted *P*-value < 0.05 were considered enriched for DEGs. Results were visualized using Cytoscape (Shannon *et al.*, 2003). The web-accessible program DAVID (https://david.ncifcrf.gov/) was used to determine enriched pathways (Benjamini-Hochberg adjusted *P*-value < 0.05) from the overlapping DEGs between our study and the study by Martin *et al.* (2017) (Huang da *et al.*, 2009*a*, *b*). Protein-protein interactions were determined for selected DEGs using the STRINGapp in Cytoscape, allowing 50 protein interactions, including scores with a confidence of >0.7 for: databases, text mining, experiments, co-expression, co-occurrence and neighbourhood (Doncheva *et al.*, 2019).

Gene sets that were potentially modulated by miRNAs were then identified. First, the list of validated miRNA targets for each of the differentially expressed miRNAs was retrieved from miRWalk2 (Dweep *et al.*, 2011, 2014). Each gene set that was enriched for DEGs was then assessed for over-representation of miRNA targets using Fisher's exact test. Gene sets with a Benjamini-Hochberg adjusted *P*-value < 0.05 were considered enriched for validated miRNA targets.

The expression levels of selected differentially expressed miRNAs and DEGs were correlated to identify potentially important miRNA-mRNA interaction partners. Correlations were calculated using Spearman's rank correlation, statistically significant correlations (adjusted *P*-value < 0.05) of >0.5 and <–0.5 were deemed as potentially interesting interactions partners.

Real-time quantitative PCR analysis

Messenger RNA expression levels were evaluated as described previously (Bongaarts *et al.*, 2018). Briefly, 250 ng of total RNA was reverse-transcribed into cDNA using oligo-dT primers. Real-time quantitative PCRs (RT-qPCRs) were run according to the manufacturer's instructions, on a Roche LightCycler® 480 thermocycler (Roche Applied Science) using LightCycler® 480 SYBR® Green I Master (Roche Applied Science) and primers listed in Supplementary Table 2. The expression of miRNAs was analysed using TaqMan™ miRNA assays (Applied Biosystems). cDNA was generated using the TaqMan™ miRNA reverse transcription kit (Applied Biosystems) according to the manufacturer's instructions, and the PCRs were run on a Roche LightCycler® 480 thermocycler (Roche Applied Science).

Quantification was performed using the LinRegPCR software in which linear regression on the Log (fluorescence) per cycle number data is applied to determine the amplification efficiency per sample (Ramakers *et al.*, 2003; Ruijter *et al.*, 2009). The starting concentration (predicted by the LinRegPCR prediction model) of each specific mRNA product was divided by the starting concentration of the reference gene elongation factor 1-alpha 1 (*EEF1A1*) and this ratio was compared between groups. The starting concentrations of miRNA-20a-5p, miRNA-34a-5p, miRNA-130b-3p and miRNA-181a-5p were divided by the geometric mean of the starting concentrations of reference genes [the U6B small nuclear RNA gene (*RNU6-6P*) and RNU44 (*SNORD44*)] and this ratio was compared between groups.

Immunohistochemistry

Tissue from control brain and SEGA was fixed in 10% buffered formalin and embedded in paraffin. Paraffin-embedded tissue was sectioned at 6 µm, mounted on precoated slides (StarFrost®, Waldemar Knittel) and stained with haematoxylin and eosin for the morphological evaluation. Sections of the most representative paraffin-embedded specimen of each case were used for double labelling.

Sections were deparaffinated in xylene, rinsed in ethanol (100%, 95% and 70%) and incubated for 20 min in 0.3% hydrogen peroxide (H_2O_2) in methanol to block endogenous peroxidase activity. Antigen retrieval was performed by incubating the sections in 0.1 M citrate buffer pH 6.0 at 120°C for 10 min using a pressure cooker. Sections were washed with phosphate-buffered saline (PBS, pH 7.4) and incubated with 10% normal goat serum (NGS) for 30 min at room temperature. Primary antibodies (1:200 rabbit monoclonal IgG anti-LAMTOR1, 8975, Cell Signaling) in Normal Antibody Diluent (ImmunoLogic) were incubated overnight at 4°C. After washing with PBS, sections were incubated with BrightVision poly-alkaline phosphatase (AP)-anti-rabbit (ImmunoLogic) for 30 min at room temperature. AP activity was visualized with the AP substrate kit III Vector Blue (SK-5300, Vector laboratories Inc.). To remove the first primary antibody, sections were incubated at 120°C in citrate buffer (10 mM NaCi, pH 6.0) for 10 min. Incubation with the second primary antibody (1:400 rabbit monoclonal IgG anti-phospho-ERK1/ERK2, 4370S, Cell Signaling; 1:200 rabbit monoclonal IgG anti-pS6, 4857, Cell Signaling) was performed overnight at 4°C. Sections were stained with a polymer-based peroxidase immunohistochemistry detection kit (BrightVision plus kit, ImmunoLogic) according to the manufacturer's instructions. Staining was performed using 3-amino-9-ethyl carbazole (AEC, Sigma-Aldrich) in 0.05 M saline buffer pH 4.9 with 0.01% H_2O_2.

Astrocyte and SEGA cell cultures

Primary foetal astrocyte-enriched cell cultures were obtained from human foetal brain tissue (14–19 gestational weeks) obtained from medically induced abortions. All material was collected from donors from whom written informed consent for the use of the material for research purposes had been obtained by the Bloemenhove clinic. Tissue was obtained in accordance with the Declaration of Helsinki and the Amsterdam UMC (location AMC) Research Code provided by the Medical Ethics Committee of the AMC. The SEGA cell culture was derived from surgical brain specimen obtained from one TSC patient (age at surgery: 25; gender: female; mutation: *TSC1*) undergoing surgery at Medical University of Vienna (Austria). Primary foetal astrocyte-enriched cell cultures and the primary SEGA culture were prepared as previously described (van Scheppingen *et al.*, 2016, 2018). Briefly, visible blood vessels were removed, after which the tissue was mechanically minced into smaller fragments and enzymatically digested at 37°C for 30 min with 2.5% trypsin (Sigma-Aldrich). Tissue was washed with incubation medium consisting of Dulbecco's modified Eagle medium (DMEM)/HAM F10 (1:1) medium (Gibco, Life Technologies), supplemented with 50 units/ml penicillin, 50 µg/ml streptomycin, and 10% foetal calf serum (Gibco, Life Technologies) and passed through a 70-µm mesh filter. The cell suspension was incubated at 37°C, 5% CO_2 for 48 h to allow time for glial cells to adhere to the culture flask and was then washed with PBS to remove excess of myelin and cell debris. Cultures were subsequently refreshed twice a week with incubation medium.

Transfection and treatment of cell cultures

SEGA cells were plated and stimulated with a final concentration of 5 µM U0126 (Sigma-Aldrich), 0.1 µM rapamycin (LC Laboratories) in dimethyl sulphoxide (DMSO) (0.05% final DMSO concentration) or vehicle (0.05% DMSO) for 24 h. Primary astrocyte cells were transfected with mimic pre-miRNA for miRNA-20a-5p (mirVana miRNA mimics, Applied Biosystems) using Lipofectamine® 2000 transfection reagent (Life Technologies) in a final concentration of 50 nM for 24 h. Cells treated with Lipofectamine® without mimic were used as a control.

Western blot analysis

Western blot analysis was performed as described previously (Korotkov *et al.*, 2018). Equal amounts of proteins (10 µg/lane for cell culture samples or 20 µg/lane for tissue samples) were separated using sodium dodecylsulfate-polyacrylamide gel electrophoresis (SDS-PAGE). Blots were blocked for 1 h in either 1% bovine serum albumin (BSA) or 5% non-fat dried milk in Tris-buffered saline-Tween (TBS-T: 20 mM Tris, 150 mM NaCl, 0.1% Tween 20, pH 7.5). Blots were incubated overnight at 4°C with primary antibodies for LAMTOR1 (1:200 mouse monoclonal, clone SL-1 IIIC4, EMD Millipore), ERK1/ERK2 (1:1500 rabbit monoclonal IgG, 9102S, Cell Signaling), phospho-ERK1/ERK2 (1:1500 rabbit monoclonal IgG, 4370S, Cell Signaling), S6 (1:1000 rabbit monoclonal IgG, 2217, Cell Signaling), pS6 (1:1000 rabbit monoclonal IgG, 4857, Cell Signaling) or β-tubulin (1:30 000 monoclonal mouse, Sigma-Aldrich). After washing with TBS-T, blots were incubated for 1 h with secondary antibodies: goat anti-mouse IgG1 or goat anti-rabbit IgG1 coupled to horseradish peroxidase (both 1:2500; Dako). Immunoreactivity was visualized using ECL western blotting detection reagent (GE Healthcare Europe). Chemiluminescent signal was detected using ImageQuant LAS 4000 analyzer (GE Healthcare). Precision Plus Protein™ Dual Color Standards (Bio-Rad) were used to determine the molecular weight of the proteins. Optical density of each band was measured using ImageJ (Adobe Photoshop CS5, San Jose, CA, USA). For each sample the optical density was calculated relative to the optical density of β-tubulin.

Proliferation assay

Proliferation of cell cultures was determined 24 h after treatment by flow cytometric cell cycle analysis as previously described (Bongaarts *et al.*, 2018; van Scheppingen *et al.*, 2018). Briefly, 24 h after treatment cells were suspended in PBS/1% BSA and stained with Fixable Viability Dye eFluor® 780 (eBioscience) on ice for 30 min. After fixation in 90% ethanol, cells were washed twice with PBS, resuspended in PBS containing 1 mg/ml propidium iodide and 1 g/ml RNase A and incubated for 10 min at 37°C. Cell cycle analysis was

performed using a FACSCanto Flow Cytometer equipped with FACSDiva software (BD Biosciences) and data analysis was performed using FlowJo 7.6 (FlowJo LLC, Ashland, OR, USA). Viable cells showing a DNA content between G1 and G2 (S-phase) were selected as proliferative population.

Statistical analysis

Statistical analysis was performed with GraphPad Prism software (Graphpad software Inc., La Jolla, CA) using the non-parametric Mann-Whitney U-test or, for multiple groups, the non-parametric Kruskal-Wallis test followed by Mann-Whitney U-test. Correlations were assessed with R using the Spearman's rank correlation test. An adjusted P-value < 0.05 was considered statistically significant.

Data availability

The data that support the findings of this study are openly available on the European Genome-phenome Archive (EGA), which is hosted by the EBI and the CRG, under the accession number: EGAS00001003787.

Results

The protein-coding transcriptome of SEGAs

To characterize the transcriptome profile of SEGAs RNA-Seq was performed on total RNA extracted from SEGA samples and control brain samples. The analysis included 19 SEGA samples from 17 TSC patients and two patients with no other signs of TSC (all surgical specimens) and eight area-matched periventricular controls (autopsy specimens) without a history of seizures or other neurological disease (see 'Materials and methods' section and Table 1). After quality assessment and filtering, ~37 million paired-end reads remained per sample, of which ~88% mapped to the GRCh38 reference genome. A principal component analysis (PCA) revealed that the major source of variability in gene expression was the diagnosis (SEGA or control; Fig. 1A) , which was confirmed by a Spearman's correlation matrix of the gene expression showing that the control samples and SEGA samples clustered separately (Fig. 1B). No specific clustering was seen based on the TSC mutation (Fig. 1B). To assess other potential confounders on the transcriptome profile of the samples a principal variance component analysis (PVCA) was performed. When all control and SEGA samples were assessed, as expected, the major contributor to the variance between the samples was the diagnosis (Supplementary Fig. 1A). Assessment of clinical features such as, mutation, age, gender, brain area, drug-treatment, mTORC1 inhibitors, epilepsy, presence of other TSC lesions or country of origin demonstrated that no single variable or two-way interaction was a single major contributor to the variance seen in the transcriptome profiles of the SEGAs (Supplementary Fig. 1B).

Differential gene expression analysis revealed 9400 DEGs (adjusted $P < 0.05$) in SEGA compared to control tissue, of which 4621 genes were overexpressed and 4779 under-expressed (Fig. 1C and Supplementary Table 3). Among the 9400 DEGs we identified 7196 protein-coding genes, 360 long non-coding RNAs, 309 pseudogenes, 1516 genes of which the biotype could not be determined by BioMart and 19 genes that could not be linked to a specific category (Supplementary Table 3). To compare the *TSC1* mutated SEGA samples with the *TSC2* mutated SEGA samples, two differential gene expression analyses were carried out: *TSC1* mutated SEGAs compared to control (*TSC1*-control) and *TSC2* mutated SEGAs compared to control (*TSC2*-control). The majority of the DEGs in both groups (*TSC1*-control and *TSC2*-control) were overlapping (5292 genes), whereas 721 genes were only found differentially expressed in *TSC1*-control and 2816 genes in *TSC2*-control (Fig. 1D). Furthermore, the fold changes between *TSC1*-control and *TSC2*-control showed a strong positive correlation (Spearman's correlation, rho = 0.89, $P < 0.01$).

To understand the organization of the protein-coding transcriptome of SEGAs better, a gene set enrichment analysis (GSEA; see 'Materials and methods' section) was performed, identifying 145 pathways enriched in SEGA compared to control tissue (adjusted $P < 0.05$). A Fisher's exact test revealed 92 pathways (adjusted $P < 0.02$) enriched for DEGs (adjusted $P < 0.05$; Fig. 1E and Supplementary Table 5). The SEGA transcriptome profile was associated with pathways including immune system, extracellular matrix organization, metabolism and the MAPK family signalling cascades. These pathways were also found among the top 25 pathways containing the highest amount of DEGs (Fig. 1F). Furthermore, most of the enriched pathways contained more overexpressed genes then under-expressed genes (Fig. 1F and Supplementary Table 5).

Previously, Martin *et al.* (2017) performed RNA-Seq on 13 SEGA samples, two subependymal nodules and eight normal brain tissue samples. To assess the robustness of our analysis, we overlapped our DEGs set with that of Martin *et al.* (2017) and performed a pathway analysis (Supplementary Fig. 2A and B). We identified 619 overexpressed genes and 777 under-expressed genes in common between both studies, resulting in 32 enriched pathways (Supplementary Fig. 2C). As the MAPK pathway was identified in all pathway analyses performed we decided to focus on this pathway for further analysis.

Higher expression of *LAMTOR* genes in SEGA compared to control tissue

Previous studies have shown that the Ragulator complex (formed by LAMTOR1, LAMTOR2, LAMTOR3, LAMTOR4 and LAMTOR5) localizes to the late

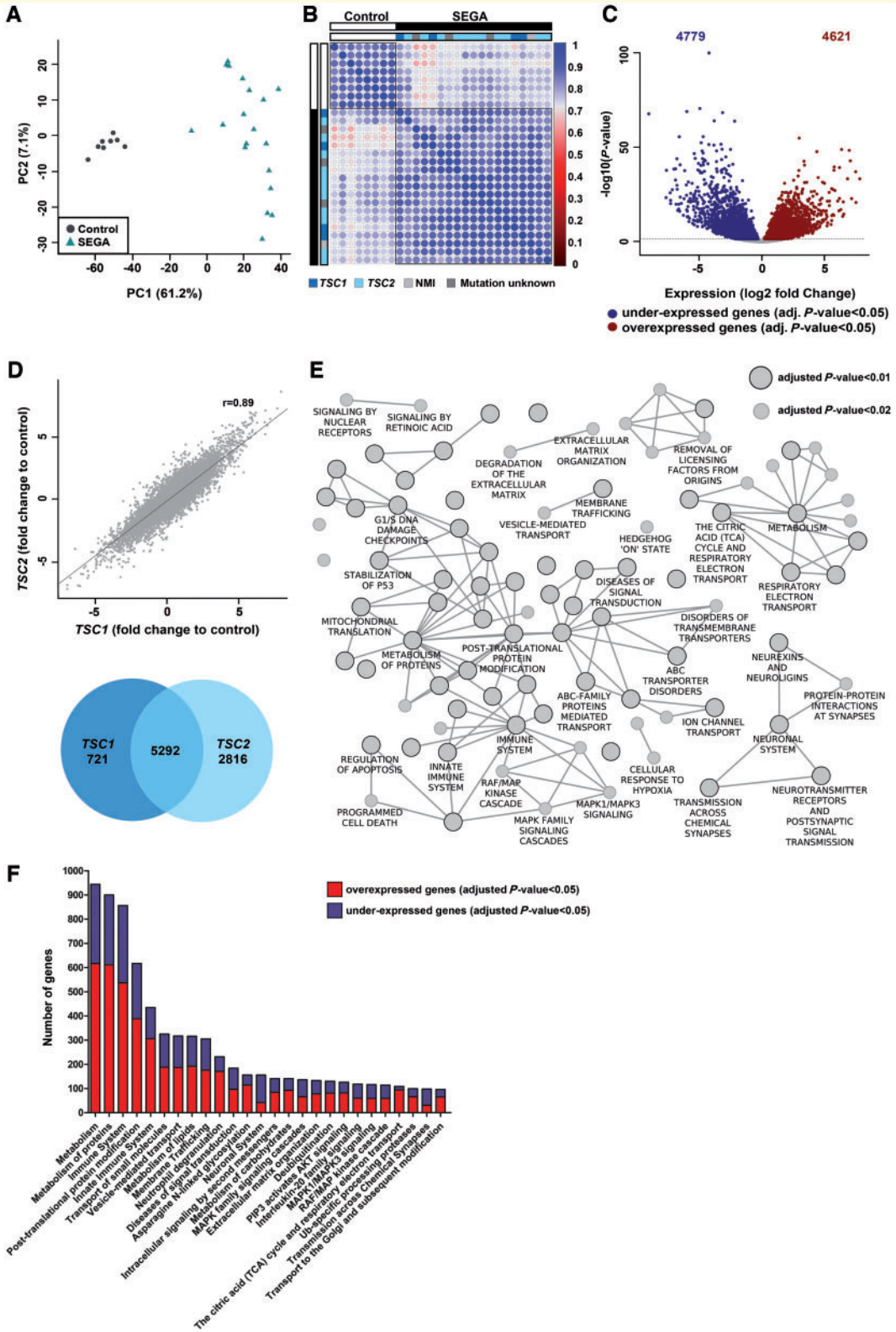

Figure 1 The protein-coding transcriptome of SEGAs. (**A**) A principal component analysis (PCA) of the RNA-Seq data in SEGA (n = 19) and periventricular control tissue (n = 8) showing that the major source of variability in gene expression is the diagnosis. x-axis: the first principal component (PC); y-axis: the second PC. (**B**) Spearman's rank correlation matrix of the RNA-Seq data showing separate clustering of SEGAs from control tissue. The scale bar indicates the strength of the correlation with 1 indicating a strong positive correlation (dark blue) and 0 indicating no correlation (dark red) between samples. (**C**) Volcano plot showing the DEGs (adjusted $P < 0.05$) between SEGAs and control tissue. A total of 4621 mRNAs were found to be overexpressed and 4779 under-expressed in SEGA compared to control tissue. (**D**) Spearman's rank correlation of the fold changes from *TSC1* mutated SEGAs compared to the fold changes from *TSC2* mutated SEGAs showing a strong correlation (rho =

(continued)

endosomes/lysosomes membrane, where it can activate both the MAPK/ERK pathway and the mTORC1 pathway (Teis *et al.*, 2002; Bar-Peled *et al.*, 2012; Nada *et al.*, 2014; Rebsamen *et al.*, 2015; de Araujo *et al.*, 2017) (Fig. 2A). Based on our RNA-Seq data we found this complex to be overexpressed in SEGA compared to control (Supplementary Table 3). RT-qPCR was used to validate the RNA-Seq data for *LAMTOR1*, *LAMTOR2*, *LAMTOR3*, *LAMTOR4* and *LAMTOR5*. All five genes were found to have higher expression in SEGA compared to control tissue (*LAMTOR1*: $P = 0.001$, *LAMTOR2*: $P = 0.0011$, *LAMTOR3*: $P = 0.006$, *LAMTOR4*: $P = 0.0325$ and *LAMTOR5*: $P = 0.0026$; Fig. 2B–F). A protein-protein interaction network for the Ragulator complex was assembled using the STRINGapp in Cytoscape and demonstrated that this complex interacts with proteins related to the MAPK/ERK pathway, including MAPK1 (ERK2), MAPK3 (ERK1), RAF1 and BRAF, as well as with proteins related to the mTORC1 pathway, including RAPTOR, MTOR, TSC1, TSC2 (Fig. 2G). Furthermore, most of these interacting proteins in the wider network were found to be differentially expressed in the RNA-Seq data and/or belonged to at least one of the enriched pathways (Fig. 2G).

ERK is activated in SEGA tissue and co-expressed with LAMTOR1

We next determined whether ERK was activated in SEGA compared to periventricular control tissue by evaluating the phosphorylation of ERK1/ERK2 (pERK). Western blotting showed higher ERK phosporylation in SEGA samples ($n = 6$; including three SEGAs with evidence of loss of heterozygosity) compared to control ($n = 4$; Mann-Whitney U-test, $P < 0.01$; Fig. 3A and B). Furthermore, no difference in pERK was seen between *TSC1* ($n = 3$) and *TSC2* ($n = 3$) mutated SEGAs. Activity of ERK was also seen in tubers ($n = 4$) and angiomyolipoma ($n = 1$), but not in control cortex ($n = 1$) or control kidney tissue ($n = 1$; Fig. 3C). LAMTOR1 was present in SEGA samples but not detected in control tissue (Mann-Whitney U-test, $P < 0.01$; Fig. 3A and B). Although variable, weak expression of LAMTOR1 was seen in cortex control, two tubers and kidney control but not in the angiomyolipoma (Fig. 3C). The cellular distribution of LAMTOR1-LAMTOR5 was assessed in SEGA ($n = 6$) and periventricular tissue ($n = 5$) using immunohistochemistry (Fig. 3D and E). In control tissue a low to weak expression of LAMTOR1-LAMTOR5 was seen mainly in the ependymal lining of lateral ventricles (red arrows). Furthermore, expression of LAMTOR1-LAMTOR5 was seen in neurons of cortex tissue (Supplementary Fig. 4, arrowheads). Both pERK and pS6 were not detected in control tissue (Fig. 3D, E and Supplementary Fig. 4). In SEGA high expression of LAMTOR1-LAMTOR5 was seen in giant cells (Fig. 3D, E, arrows and insets). Furthermore, LAMTOR1-LAMTOR5 were co-expressed in cells with pERK (mainly nuclear) and pS6 (mainly cytoplasmic).

Inhibition of ERK with U0126 decreases the proliferation of primary SEGA cells

We further evaluated the role of ERK in the cell cycle progression of SEGA cells using flow cytometric cell cycle analysis in one SEGA-derived cell culture (*TSC1* mutated). The viability of cells was not altered after treatment with the ERK inhibitor U0126, rapamycin or the combination of U0126 and rapamycin (Fig. 4A). The percentage of cells in the S-phase was decreased after treatment with U0126 ($P < 0.01$) or rapamycin ($P < 0.01$) compared to control (DMSO; Fig. 4A and B). Combining U0126 with rapamycin also decreased the proliferation of SEGA cells ($P < 0.01$) compared to control but not compared to U0126 or rapamycin alone. Inhibition of ERK activity by U0126 was confirmed by western blotting as well as the inhibition of mTORC1 pathway by rapamycin using pS6 as a readout (Supplementary Fig. 3).

The small non-coding RNA landscape of SEGAs

Small RNA-Seq was performed to detect miRNAs and other small non-coding RNAs in the same cohort of SEGA and control samples that were used for RNA-Seq. After quality assessment and filtering, ~6 million reads remained, of which 83% were successfully mapped to the human reference genome GRCh38. Differential expression testing between SEGA samples and control, identified 140 differentially expressed small RNAs of which 72 were under-expressed and 68 overexpressed (Fig. 5A and Supplementary Table 4). Among the differentially expressed small RNAs we identified one snRNA, three snoRNAs, four vtRNAs, 94 miRNAs, 15 unannotated gene derived

Figure 1 Continued
0.89, $P < 0.001$). The Venn diagram shows 5292 DEGs in common between *TSC1* and *TSC2* mutated SEGAs, 721 DEGs were specific for *TSC1* mutated SEGAs and 2816 DEGs were specific for *TSC2* mutated SEGAs. (**E**) Schematic overview using Cytoscape of pathways enriched in SEGA compared to control tissue. Geometric testing was used to determine if the amount of DEGs was significant (adjusted $P < 0.02$) per pathway. Lines indicate genes in common between pathways. (**F**) Graphical representation of overexpressed genes (red) and under-expressed genes (blue) in 25 enriched pathways containing the highest amount of DEGs.

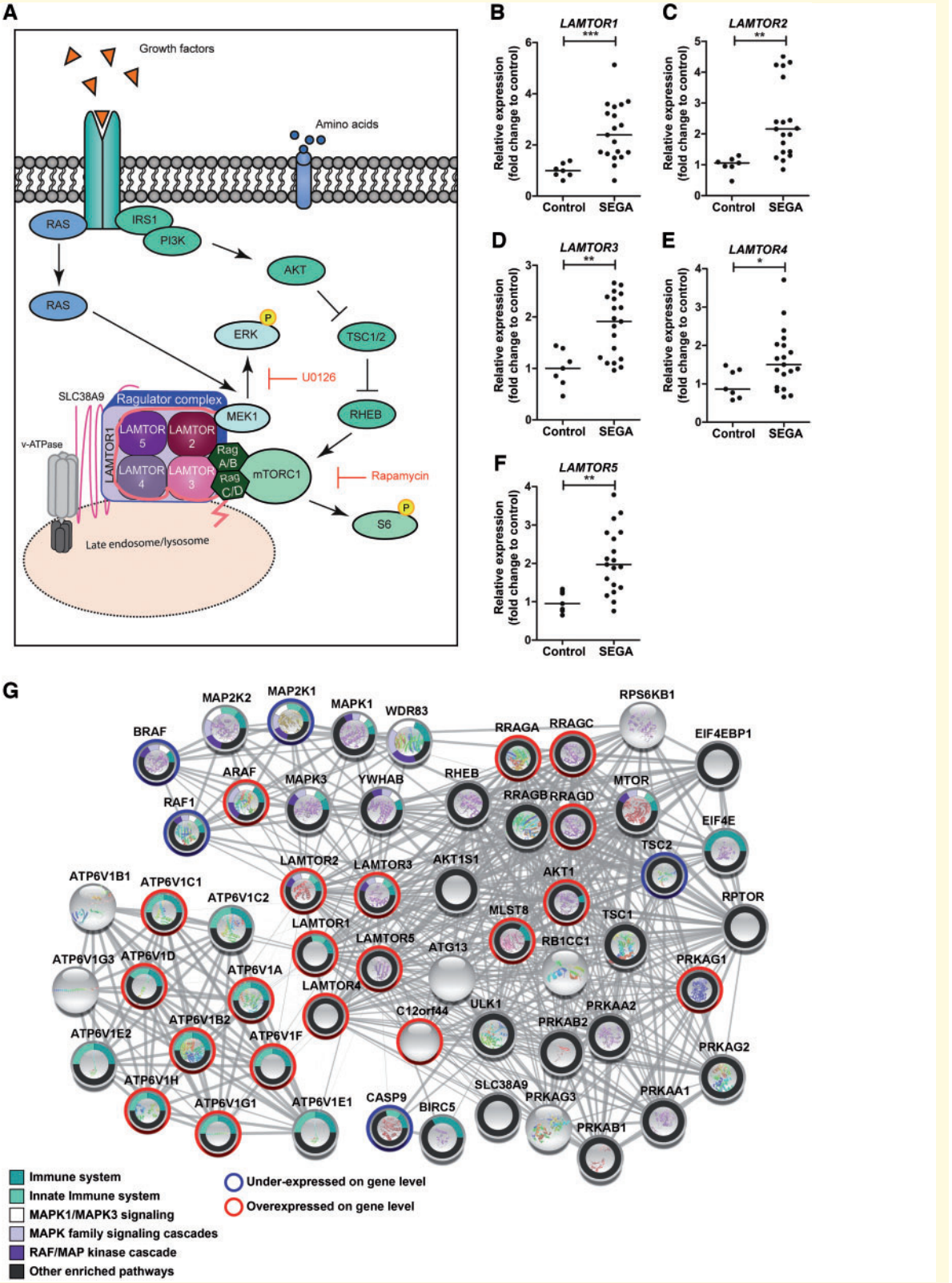

Figure 2 The Ragulator complex in SEGAs. (**A**) Schematic overview showing the Ragulator complex dependent mTORC1/MAPK signalling. Crystal structure of the Ragulator complex revealed that LAMTOR1 holds together the LAMTOR2/3 and LAMTOR4/5 heterodimers and anchors the complex to the late endosomes/lysosomes (de Araujo *et al.*, 2017). In the presence of amino acids and growth factors, the Ragulator complex can promote Rag GTPase- dependent mTORC1 activation and MEK1 dependent ERK activation via direct interaction of RagA-D and MEK1 with LAMTOR2/3 heterodimer (Teis *et al.*, 2002; Bar-Peled *et al.*, 2012). Furthermore, the Ragulator complex interacts with vacuolar H^+-ATPase and neutral amino acid transporter SLC38A9 and thereby can promote mTORC1 activation in the presence of amino acids

(continued)

small RNAs and 23 intergenic small RNAs (Fig. 5B). The majority of the differentially expressed small RNAs were miRNAs (67.2%) of which 49 were under-expressed in SEGA compared to control and 45 were miRNAs were overexpressed (Fig. 5B and C). The unannotated gene derived and intergenic small RNAs, as defined in the materials and methods, formed the second and third largest groups of differentially expressed small RNAs, respectively. Overall 16.4% of the differentially expressed small RNAs were intergenic and 10.7% were gene derived.

Next we analysed which miRNAs could interact with the 92 enriched pathways from GSEA by assessing each pathway using a Fisher's exact test, for an over-representation of validated miRNA targets of each differentially expressed miRNA. A total of 81 pathways were found to be enriched for validated targets of 45 of the differentially expressed miRNAs (Fisher's exact test, adjusted $P < 0.05$; Fig. 5D). miRNA-20a-5p, miRNA-34a-5p, miRNA-130b-3p and miRNA-181a-5p were selected for validation using RT-qPCR and were found differentially expressed in accordance with the RNA-Seq data (Fig. 5E).

To identify miRNAs that could target one or more of *LAMTOR1*, *LAMTOR2*, *LAMTOR3*, *LAMTOR4* or *LAMTOR5*, differentially expressed miRNAs were evaluated with miRWalk2. *LAMTOR1* was found to be a validated target of miRNA-20a-5p and let-7c-5p, *LAMTOR3* was found to be a validated target of miRNA-362-3p and miRNA-548ba and *LAMTOR5* was found to be a validated target of miRNA-221-3p and miRNA-501-5p. Spearman correlations using the RNA-Seq data were calculated between each miRNA and their validated identified target. This analysis identified miRNA-20a-5p (adjusted $P = 0.012$, rho = –0.55) and miRNA-221-3p (adjusted $P = 0.015$, rho = 0.51) as potentially interesting regulatory partners of *LAMTOR1* and *LAMTOR5* respectfully. Based on these results miRNA-20a-5p was selected for further analysis. Transfection of primary foetal astrocytes with miRNA-20a-5p mimic showed that miRNA-20a-5p could downregulate *LAMTOR1* ($P = 0.0022$), *LAMTOR2* ($P = 0.0087$) and *LAMTOR5* ($P = 0.026$), but not *LAMTOR3* ($P = 0.4848$) or *LAMTOR4* ($P = 0.0649$; Fig. 6).

Discussion

In this study we performed parallel sequencing of the coding and non-coding transcriptome of SEGAs from TSC patients. Among the differentially expressed protein-coding genes we identified an enrichment for genes related to the MAPK pathway. ERK activation in SEGA was confirmed on protein level and was also found in tubers. Both the ERK inhibitor U0126 and rapamycin were able to decrease the proliferation of SEGA cells of one SEGA-derived cell culture *in vitro*. Additionally, we showed that genes related to the Ragulator complex, a complex activating both the MAPK/ERK and mTORC1 pathway, were overexpressed in SEGA compared to control tissue. Therefore, we provide initial evidence of linkage between these two important pathways of tumour growth and cell survival.

In the present study, high-throughput sequencing of both coding and non-coding transcriptome was performed on 19 SEGAs and eight periventricular control tissue. We identified substantial gene expression changes in SEGAs compared to periventricular control tissue. These gene expression changes appear to be independent of the *TSC1/TSC2* mutation or other clinical information available. Pathway enrichment analysis identified 116 pathways enriched in SEGA compared to control tissue, including immune system, extracellular matrix organization, metabolism, transmission across chemical synapses and the MAPK family signalling cascades. Several of the enriched pathways found in our study are related to the biological processes found in previous transcriptome-based SEGA studies (Tyburczy *et al.*, 2010; Martin *et al.*, 2017). Differential expression of genes related to the immune system has also been identified in cortical tubers through the use of RNA-Seq and microarrays (Boer *et al.*, 2010; Martin *et al.*, 2017; Mills *et al.*, 2017). Multiple studies of TSC animal models and TSC human tissue, including prenatal TSC lesions have documented dysregulation of inflammation related pathways, such as immune response, suggesting that this biological process is more conserved across TSC pathology rather than a SEGA specific process (Boer *et al.*, 2008, 2010; Zurolo *et al.*, 2011; Prabowo *et al.*, 2013; Zhang *et al.*, 2015). One of the enriched pathways found in this study was the MAPK pathway. Previous studies focusing on *TSC2* mutated tubers and SEGAs in which the TSC2 protein is still present documented the presence of MAPK/ERK activation (Han *et al.*, 2004; Ma *et al.*, 2005, 2007). In accordance with these studies we show that ERK activation is present in tubers and SEGA and that the activation of ERK seen in SEGAs seems to be independent of *TSC1/TSC2* mutation and loss of

Figure 2 Continued
(Rebsamen *et al.*, 2015; Wang *et al.*, 2015). Rapamycin inhibits mTORC1, whereas U0126 inhibits the MEK1 dependent ERK activation. (**B**–**F**) RT-qPCR of *LAMTOR1* (**B**), *LAMTOR2* (**C**), *LAMTOR3* (**D**), *LAMTOR4* (**E**) and *LAMTOR5* (**F**) in SEGA ($n = 19$) compared to control tissue ($n = 8$), which together can form the Ragulator complex. Data are expressed relative to the expression observed in control tissue. $^{*}P < 0.05$, $^{**}P < 0.01$, $^{***}P < 0.001$, Mann-Whitney U-test. (**G**) A String functional protein association network of the Ragulator complex (LAMTOR1–LAMTOR5) interactions identified by StringApp for Cytoscape. High confidence interactions were selected (0.7), identifying interactions with proteins related to the MAPK/ERK and mTORC1 pathway. The outer circle indicates overexpression (red) or under-expression (blue) on RNA level based on the RNA-Seq data. The inner circle indicates to which enriched pathways each protein-interactor belongs to.

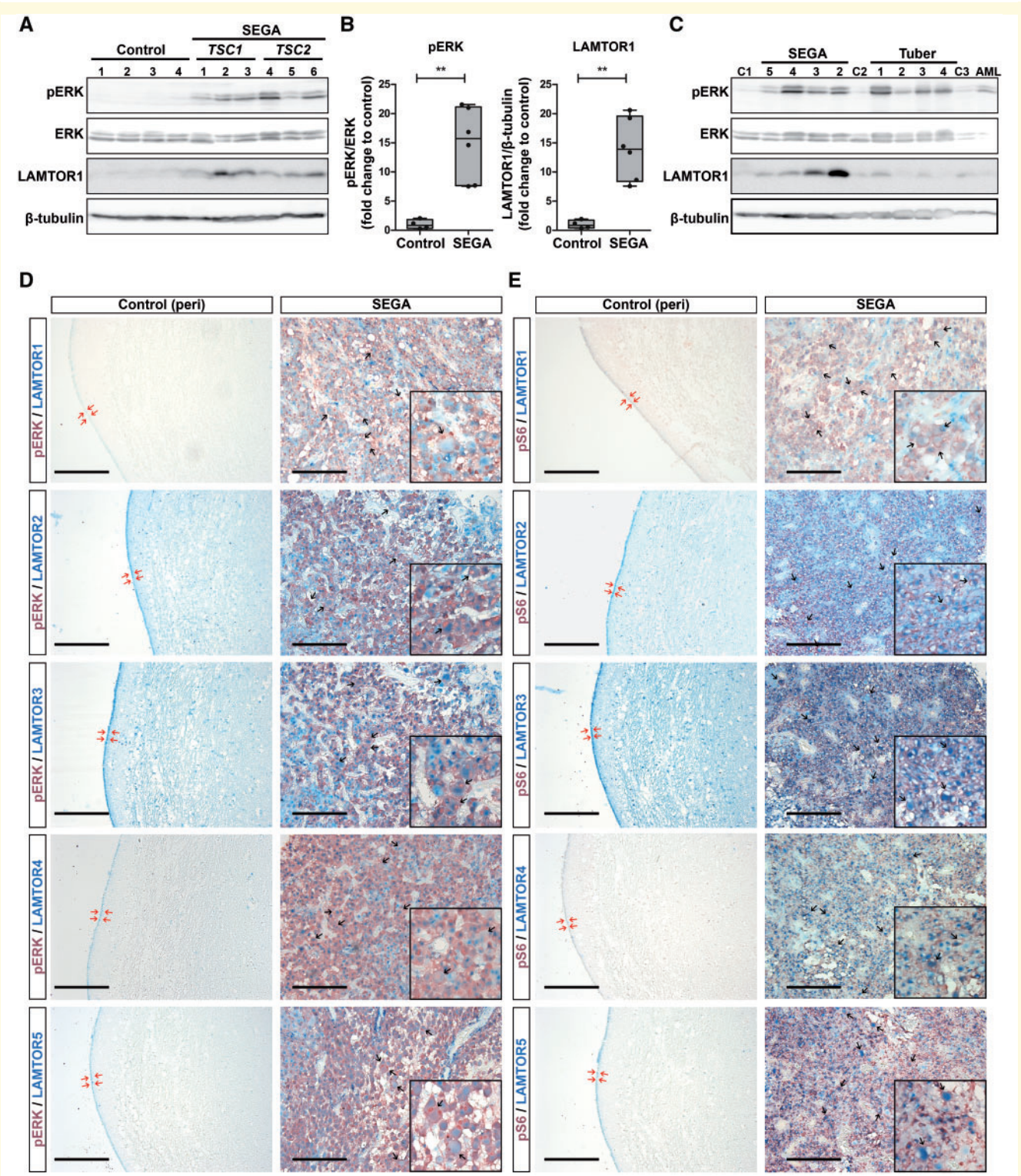

Figure 3 ERK activation and LAMTOR1-LAMTOR5 protein expression in SEGAs. (**A**) Western blot showing pERK1/2 and LAMTOR1 expression in SEGA [n = 6; *TSC1* mutated: sample 1–3 and *TSC2* mutated: samples 4–6; loss of heterozygosity: samples 3, 4 and 6; loss of heterozygosity identified as described in Bongaarts *et al.* (2017)] but not in periventricular control tissue (n = 4). β-tubulin was used as a loading control. (**B**) Quantification of pERK1/2 and LAMTOR1 signals normalized to either total ERK1/2 or β-tubulin. $^{**}P < 0.01$, Mann-Whitney U-test. (**C**) Western blot showing pERK1/2 and LAMTOR1 expression in SEGA (n = 4), cortical tubers (n = 4) and angiomyolipoma (AML; n = 1) but not in periventricular control tissue (n = 1: sample C1), cortex control (n = 1; sample C2) and normal kidney tissue (n = 1; sample C3). β-tubulin was used as a loading control. (**D** and **E**) Immunohistochemistry for pERK1/2 (red, **D**) or pS6 (red, **E**) together with LAMTOR1–LAMTOR5 (blue) on SEGA (n = 6) and periventricular control tissue (n = 5). Insets show a higher magnification of giant cells (indicated with arrows) in SEGA and red arrows indicate the ependymal lining of lateral ventricles. Scale bar = 200 μm; insets = 100 μm.

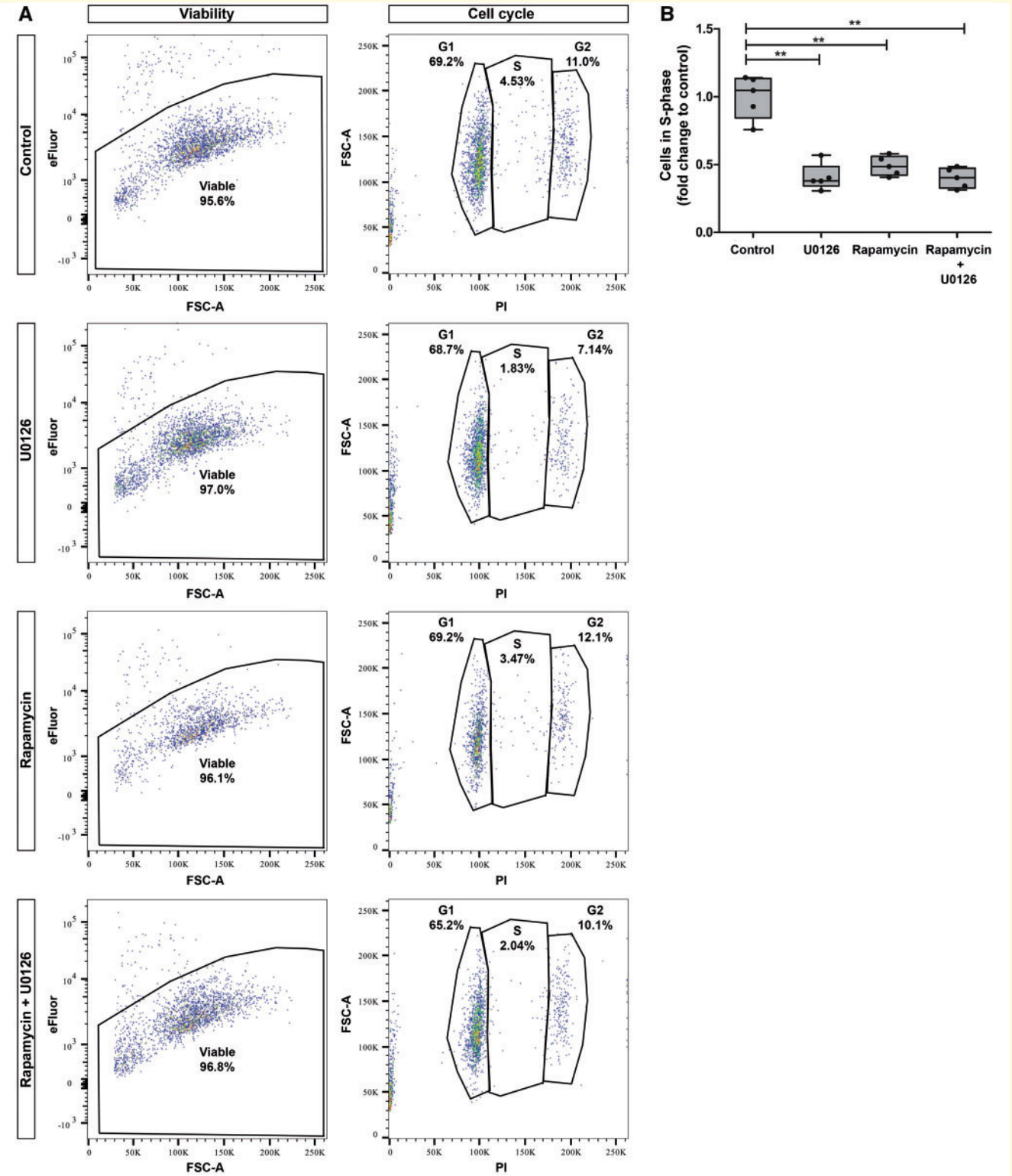

Figure 4 ERK inhibitor U0126 and rapamycin inhibit proliferation of SEGA cells *in vitro*. (**A**) Primary SEGA cells from one SEGA-derived cell culture were stimulated for 24 h with U0126 (5 μM), rapamycin (0.01 μM), a combination of rapamycin with U0126 (rapamycin + U0126) or DMSO (0.05%) as a control. Flow cytometry analysis was used to assay the viability with eFluor or the cell-cycle state using propidium iodide (PI) staining of SEGA cells (n = 5). (**B**) Quantification of the PI staining showed lesser cells in the S-phase in the U0126, rapamycin and the rapamycin + U0126 conditions compared to control (0.05% DMSO). Data are expressed relative to the control condition. $^{**}P < 0.01$, Kruskal-Wallis test followed by Mann-Whitney U-test.

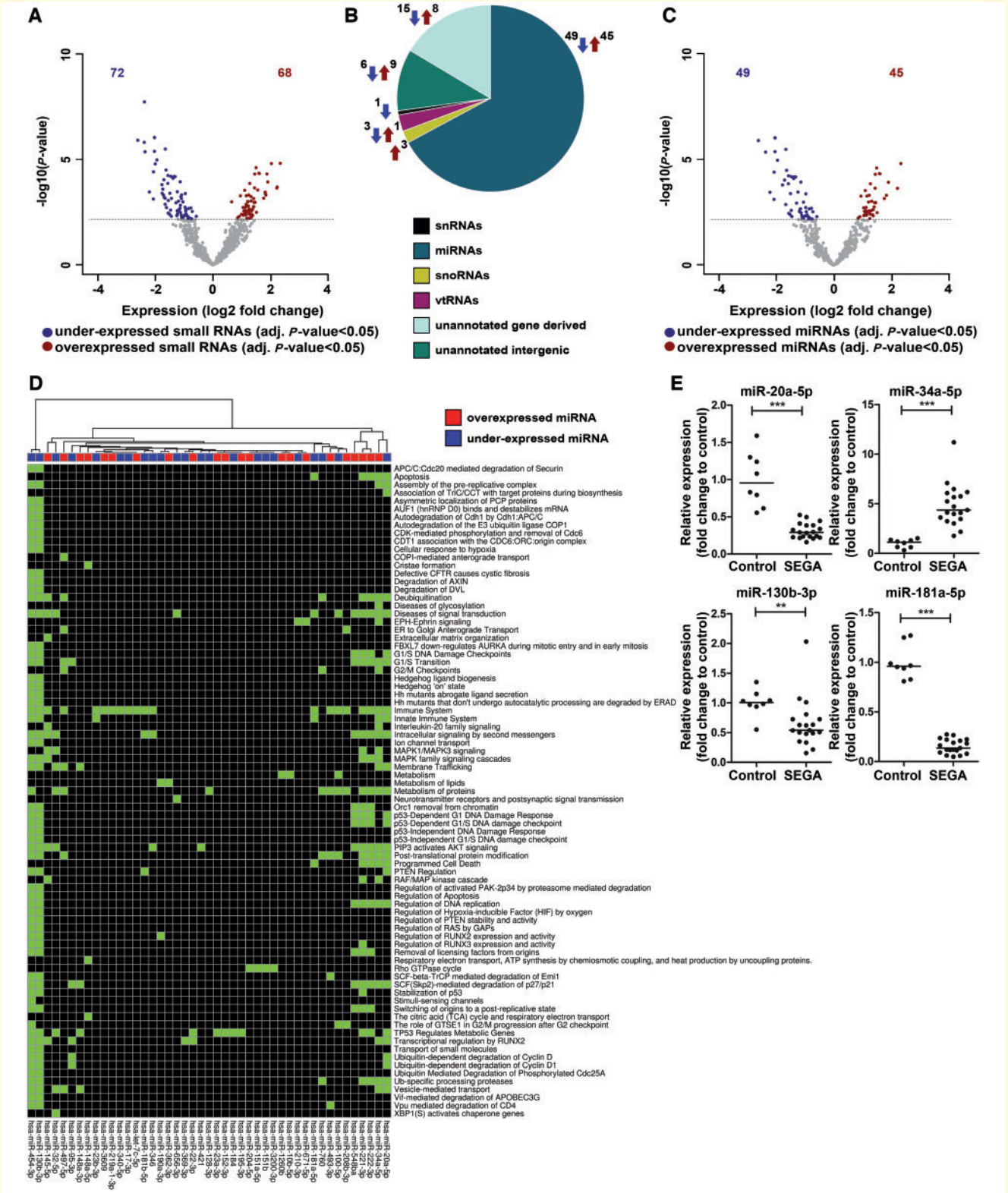

Figure 5 The small non-coding RNA landscape of SEGAs. (**A**) Volcano plot showing 72 under-expressed and 68 overexpressed small RNAs in SEGA (n = 19) compared to control tissue (n = 8; adjusted $P < 0.05$). (**B**) Pie chart showing the distribution of different small RNAs differentially expressed in SEGA compared to control. miRNA = microRNA; snRNA = small nuclear RNA; snoRNA = small nucleolar RNA; vtRNA = vault RNA. (**C**) Volcano plot showing 49 under-expressed and 45 overexpressed miRNAs in SEGA (n = 19) compared to control tissue (n = 8; adjusted $P < 0.05$). (**D**) Heat map showing 81/92 enriched pathways from GSEA that were enriched for validated targets of 45/94 of the differentially expressed miRNAs (Fisher's exact test, adjusted $P < 0.05$). Pathways enriched for a specific miRNA are indicted with a green box. (**E**) Validation of selected differentially expressed miRNAs (miRNA-20a-5p, miRNA-34a-5p, miRNA-130b-3p and miRNA-181a-5p) in SEGA (n = 19) compared to control tissue (n = 8) using TaqMan™ PCR. $^{**}P < 0.01$, $^{***}P < 0.001$, Mann-Whitney U-test.

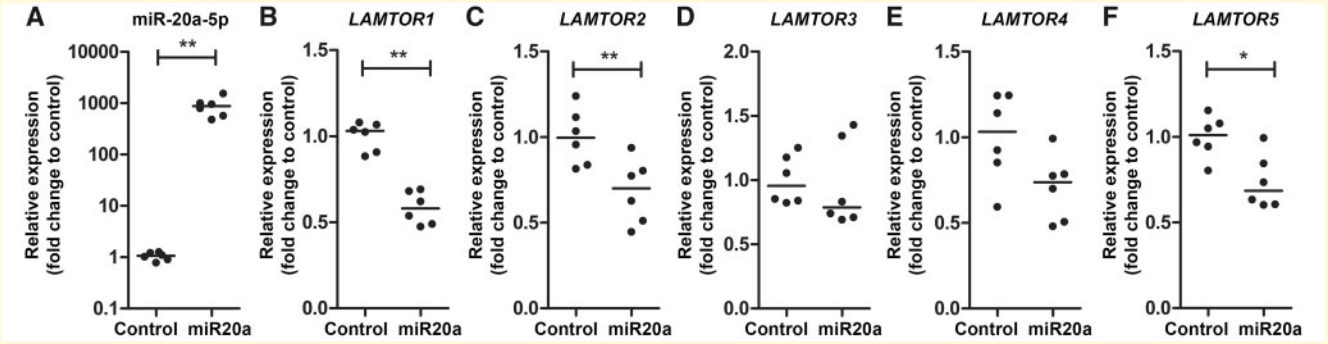

Figure 6 Relative expression of *LAMTOR* genes after transfection with miRNA-20a-5p mimic in foetal astrocytes. TaqMan™ PCR of miRNA-20a-5p (**A**) and RT-qPCR of *LAMTOR1* (**B**), *LAMTOR2* (**C**), *LAMTOR3* (**D**), *LAMTOR4* (**E**) and *LAMTOR5* (**F**) in foetal astrocytes transfected with miRNA-20a-5p mimic (miR20a) for 24h (n = 3 biological triplets and two technical duplicates). Data are normalized to Lipofectamine® (control). $^{*}P < 0.05$, $^{**}P < 0.01$, Mann-Whitney U-test.

heterozygosity. Therefore, it could be of interest to investigate the MAPK/ERK activation further in other TSC-related lesions.

Current treatment of SEGAs is limited to surgical removal and mTORC1 inhibitors, including rapamycin and everolimus (Franz *et al.*, 2006, 2013, 2014, 2015; Krueger *et al.*, 2010, 2013; Kotulska *et al.*, 2013). In recent TSC clinical trials, it was shown that responses to mTORC1 inhibitors can be variable and that lesions tend to relapse after cessation of treatment (Franz *et al.*, 2006, 2014; Bissler *et al.*, 2008; Krueger *et al.*, 2010, 2016; McCormack *et al.*, 2011; Martins *et al.*, 2013). A possible explanation for this could be that inhibition of mTORC1 leads to the disruption of the negative feedback on the MAPK/ERK pathway resulting in MAPK/ERK activation (Carracedo *et al.*, 2008; Albert *et al.*, 2009). Furthermore, MAPK/ERK activation can result in TSC2 phosphorylation and thereby increase mTORC1 activation, indicating that these two pathways are intrinsically linked (Han *et al.*, 2004; Ma *et al.*, 2005, 2007). Only two patients included in the present study were treated with mTORC1 inhibitors, indicating that the ERK activation seen cannot be explained by mTORC1 inhibition. Previous studies have shown that inhibiting MAPK/ERK activity decreased the proliferation of *Tsc2*$^{-/-}$ mouse embryonic fibroblast cells, SEGA cells and tumour growth in mice heterozygous for *Tsc2* (Govindarajan *et al.*, 2003; Mi *et al.*, 2009; Tyburczy *et al.*, 2010). In accordance with these studies, we show that inhibiting ERK in a primary human derived SEGA culture using the ERK inhibitor U0126 decreased the proliferation in a similar manner to treatment with rapamycin as a mTORC1 inhibitor alone. In contrast to previous research, we did not observe differences between rapamycin and combined therapy with rapamycin and the ERK inhibitor U0126 in SEGA cells from one SEGA-derived cell culture (Mi *et al.*, 2009; Tyburczy *et al.*, 2010). A previous study by Mi *et al.* (2009) identified that combined treatment of rapamycin and ERK inhibitors was more efficient in inhibiting the proliferation of *TSC2* deficient cells then treatment with rapamycin or ERK inhibitors alone after 3 days of treatment, but not over shorter time periods. Furthermore, Tyburczy *et al.* (2010) showed that suppression of both the mTORC1 and MAPK/ERK pathway was most efficient in decreasing proliferation after 48 h and cell viability after 3 days of treatment compared to mTORC1 or ERK inhibition alone (Tyburczy *et al.*, 2010). This suggests that combined therapy may be only beneficial over a longer period of time. However, considering the side effects, it may also be difficult to treat patients with multiple inhibitors at the same time (Sadowski *et al.*, 2016; Cheng and Tian, 2017). Therefore, therapeutic interventions resulting in decreased MAPK signalling in SEGA could be used as an alternative to the current treatments available, especially in TSC patients who do not adequately respond to mTORC1 inhibitors. However, the need for more specific treatment remains. As the MAPK/ERK pathway is known to regulate cell proliferation but has also been linked to epilepsy, patients with other TSC lesions, such as tubers, may also benefit from treatment with MAPK/ERK inhibitors; however, further investigation is highly needed (Nateri *et al.*, 2007; de Araujo Herculano *et al.*, 2011; Gorter *et al.*, 2014; Glazova *et al.*, 2015; Pernice *et al.*, 2016; Shao *et al.*, 2016).

To the best of our knowledge the mechanism that activates the MAPK/ERK pathway in SEGA and other TSC lesions has not been determined. Previous studies have demonstrated that the Ragulator complex (LAMTOR1–LAMTOR5) is involved in lysosomal positioning, autophagy and the activation of both MAPK/ERK and mTORC1 pathways in the presence of nutrients and growth factors (Teis *et al.*, 2002; Bar-Peled *et al.*, 2012; de Araujo *et al.*, 2017; Filipek *et al.*, 2017). It has been shown that the Ragulator complex is necessary for the localization and stabilization of RAG GTPases (RagA-RagD) and mTORC1 to the late endosomes/lysosomes membrane, which is required for amino acid-dependent activation of mTORC1 (Sancak *et al.*, 2010; Bar-Peled *et al.*, 2012). Furthermore, the Ragulator complex can also activate the

MAPK/ERK pathway by recruiting MEK1 to the late endosomes/lysosomes (Wunderlich *et al.*, 2001; Teis *et al.*, 2002). Although the involvement of the Ragulator complex in the mTORC1 and MAPK/ERK signalling is well established, the role of this complex in human pathology has rarely been studied. In the present study, we identified the Ragulator complex (*LAMTOR1–LAMTOR5*) to be overexpressed in SEGAs compared to control tissue. RNA-Seq on tubers did not find an overexpression of LAMTOR genes in tubers, suggesting that overexpression of this complex is unique to SEGA (Martin *et al.*, 2017; Mills *et al.*, 2017). While we found weak expression of LAMTOR1 in a subset of tubers, expression of LAMTOR1 was also seen in neurons of healthy control tissue, which could explain why no difference was found on RNA level between tubers and cortex control in previous studies (Martin *et al.*, 2017; Mills *et al.*, 2017). Furthermore, we show that LAMTOR1–5 co-express with pERK and pS6 suggesting that the Ragulator complex might be involved with the activation of these two pathways in SEGA and could be an interesting target for therapy. However, further research is needed to show the direct link between the Ragulator complex and SEGA development.

So far, research on small non-coding RNAs in SEGA has been limited to miRNA expression using microarray analysis or direct RT-qPCR (Ames *et al.*, 2017; Bongaarts *et al.*, 2018). In this study we mapped the whole small non-coding RNA profile in SEGAs relative to control tissue and found that miRNAs, snRNAs, snoRNAs and vtRNAs were amongst the differentially expressed small RNAs. We identified miRNAs as the largest group of differentially expressed small RNAs. As miRNAs are known regulators of gene expression we used a bioinformatics approach to identify miRNAs that could potentially modulate the enriched pathways found in this study. In doing so, we identified miRNA-20a-5p as a potential regulator of several *LAMTOR* genes. We also identified a high number of unannotated small transcripts. Although these unannotated small RNAs still need to be validated and functionally characterized, they could potentially harbour novel small RNAs and therefore be interesting for further research.

Taken together, this study shows activation of ERK in SEGAs and suggests that the MAPK/ERK pathway could be used as a target for treatment independent of, or in combination with mTORC1 inhibitors for TSC patients with SEGAs. Furthermore, we are the first to identify the overexpression of the Ragulator complex in human pathology, linking the constitutive activated mTORC1 pathway and MAPK/ERK activation seen in SEGAs, highlighting the Ragulator complex as a promising novel therapeutic target.

Acknowledgements

The authors thank all supporters of the TSC brain bank (Laboratory of Molecular and Cellular Neurobiology, International Institute of Molecular and Cell Biology, Warsaw, Poland: J. Jaworski, A Tempes; The Service d'Anatomie Pathologique, CHI de Creteil and Inserm U676, Hospital Robert Debre, Paris, France: H. Adle-Biassette; Department of Pediatrics, Institute of Neurology, Department of Neurosurgery, Medical University Vienna, Austria: M. Feucht, T. Scholl, J. Hainfellner, T. Czech; Department of Neurology and Pathology and Molecular Medicine, Charles University, 2nd Faculty of Medicine, Motol University Hospital, Prague, Czech Republic: P. Krsek, J. Zamecnik; Department of Neuropathology, John Radcliffe Hospital, Oxford, UK: C. Kennard; Department of Anatomic Pathology Sciences, Università Sapienza, Rome, Italy: M. Antonelli, F. Giangaspero; Insitute of Neuropathology, Westfälische Wilhelms – Universität Münster, Münster, Germany: W. Paulus, M. Hasselblatt; Department of Neuropathology, University Hospital Erlangen, Erlangen, Germany: R. Coras, I. Blümcke; Bethel Epilepsy Centre, Bielefeld, Germany: T. Polster, C.G. Bien; Laboratory of Neuropathology, Department of Neurology, Hospital de Santa Maria (CHLN), Lisbon, Portugal: J. Pimentel; Department of Human Pathology and Oncology, University of Florence and Division of Neurosurgery, 'Anna Meyer' Pediatric Hospital, Florence, Italy: A. M. Buccoliero, F. Giordano; Department of Pathology, Faculty of Medicine, Hacettepe University, Ankara, Turkey: F. Söylemezoğlu). In this regard we would like to acknowledge all personnel involved in sending us the material. Furthermore, the authors would like to thank Dr Mark Nellist (Department of Clinical Genetics, Erasmus Medical Centre, Rotterdam, The Netherlands) and Dr David J. Kwiatkowski, MD, PhD (Division of Experimental Medicine and Medical Oncology, Brigham and Women's Hospital, Boston, USA) for performing *TSC1/TSC2* mutation analysis.

Funding

This work was supported by KIKA (Stichting Kinderen Kankervrij; A.B., A.M., B.S., E.A.); Stichting AMC Foundation (E.A.); Stichting TSC Fonds (E.A.); the Austrian Science Fund (FWF, no. J3499; A.M.); the European Union 7th framework program: acronym EPISTOP (grant agreement no. 602391; J.S., F.J., T.S., S.J., M.F., A.M., E.A.); the European Union 7th framework program: acronym DESIRE (grant agreement no. 602531; I.B.); the Polish Ministerial funds for science (Years 2013–2018) for the implementation of international co-financed project (K.K., S.J.) and internal research project of the Children's Memorial Health Institute no.S132/2013 (K.K., S.J.).

Competing interests

The authors report no competing interests. We confirm that we have read the Journal's position on issues involved in

ethical publication and affirm that this report is consistent with those guidelines.

Supplementary material

Supplementary material is available at *Brain* online.

References

Adriaensen ME, Schaefer-Prokop CM, Stijnen T, Duyndam DA, Zonnenberg BA, Prokop M. Prevalence of subependymal giant cell tumors in patients with tuberous sclerosis and a review of the literature. Eur J Neurol 2009; 16: 691–6.

Albert L, Karsy M, Murali R, Jhanwar-Uniyal M. Inhibition of mTOR activates the MAPK pathway in Glioblastoma multiforme. Cancer Genomics Proteomics 2009; 6: 255–61.

Ames HM, Yuan M, Vizcaino MA, Yu W, Rodriguez FJ. MicroRNA profiling of low-grade glial and glioneuronal tumors shows an independent role for cluster 14q32.31 member miR-487b. Mod Pathol 2017; 30: 204–16.

Aronica E, Becker AJ, Spreafico R. Malformations of cortical development. Brain Pathol 2012; 22: 380–401.

Aronica E, Crino PB. Epilepsy related to developmental tumors and malformations of cortical development. Neurotherapeutics 2014; 11: 251–68.

Bar-Peled L, Schweitzer LD, Zoncu R, Sabatini DM. Ragulator is a GEF for the rag GTPases that signal amino acid levels to mTORC1. Cell 2012; 150: 1196–208.

Bissler JJ, McCormack FX, Young LR, Elwing JM, Chuck G, Leonard JM, et al. Sirolimus for angiomyolipoma in tuberous sclerosis complex or lymphangioleiomyomatosis. N Engl J Med 2008; 358: 140–51.

Boer K, Crino PB, Gorter JA, Nellist M, Jansen FE, Spliet WG, et al. Gene expression analysis of tuberous sclerosis complex cortical tubers reveals increased expression of adhesion and inflammatory factors. Brain Pathol 2010; 20: 704–19.

Boer K, Jansen F, Nellist M, Redeker S, van den Ouweland AM, Spliet WG, et al. Inflammatory processes in cortical tubers and subependymal giant cell tumors of tuberous sclerosis complex. Epilepsy Res 2008; 78: 7–21.

Bolger AM, Lohse M, Usadel B. Trimmomatic: a flexible trimmer for Illumina sequence data. Bioinformatics 2014; 30: 2114–20.

Bongaarts A, Giannikou K, Reinten RJ, Anink JJ, Mills JD, Jansen FE, et al. Subependymal giant cell astrocytomas in Tuberous sclerosis complex have consistent TSC1/TSC2 biallelic inactivation, and no BRAF mutations. Oncotarget 2017; 8: 95516–29.

Bongaarts A, Prabowo AS, Arena A, Anink JJ, Reinten RJ, Jansen FE, et al. MicroRNA519d and microRNA4758 can identify gangliogliomas from dysembryoplastic neuroepithelial tumours and astrocytomas. Oncotarget 2018; 9: 28103–15.

Carracedo A, Ma L, Teruya-Feldstein J, Rojo F, Salmena L, Alimonti A, et al. Inhibition of mTORC1 leads to MAPK pathway activation through a PI3K-dependent feedback loop in human cancer. J Clin Invest 2008; 118: 3065–74.

Chan JA, Zhang H, Roberts PS, Jozwiak S, Wieslawa G, Lewin-Kowalik J, et al. Pathogenesis of tuberous sclerosis subependymal giant cell astrocytomas: biallelic inactivation of TSC1 or TSC2 leads to mTOR activation. J Neuropathol Exp Neurol 2004; 63: 1236–42.

Cheng Y, Tian H. Current development status of MEK inhibitors. Molecules 2017; 22: 1551.

Croft D, O'Kelly G, Wu G, Haw R, Gillespie M, Matthews L, et al. Reactome: a database of reactions, pathways and biological processes. Nucleic Acids Res 2011; 39: D691–7.

Cuccia V, Zuccaro G, Sosa F, Monges J, Lubienieky F, Taratuto AL. Subependymal giant cell astrocytoma in children with tuberous sclerosis. Childs Nerv Syst 2003; 19: 232–43.

de Araujo Herculano B, Vandresen-Filho S, Martins WC, Boeck CR, Tasca CI. NMDA preconditioning protects against quinolinic acid--induced seizures via PKA, PI3K and MAPK/ERK signaling pathways. Behav Brain Res 2011; 219: 92–7.

de Araujo MEG, Naschberger A, Furnrohr BG, Stasyk T, Dunzendorfer-Matt T, Lechner S, et al. Crystal structure of the human lysosomal mTORC1 scaffold complex and its impact on signaling. Science 2017; 358: 377–81.

de Ribaupierre S, Dorfmuller G, Bulteau C, Fohlen M, Pinard JM, Chiron C, et al. Subependymal giant-cell astrocytomas in pediatric tuberous sclerosis disease: when should we operate? Neurosurgery 2007; 60: 83–9; discussion 9–90.

Dibble CC, Elis W, Menon S, Qin W, Klekota J, Asara JM, et al. TBC1D7 is a third subunit of the TSC1-TSC2 complex upstream of mTORC1. Mol Cell 2012; 47: 535–46.

DiMario FJ Jr. Brain abnormalities in tuberous sclerosis complex. J Child Neurol 2004; 19: 650–7.

Doncheva NT, Morris JH, Gorodkin J, Jensen LJ. Cytoscape StringApp: network analysis and visualization of proteomics data. J Proteome Res 2019; 18: 623–32.

Dweep H, Gretz N, Sticht C. miRWalk database for miRNA-target interactions. Methods Mol Biol 2014; 1182: 289–305.

Dweep H, Sticht C, Pandey P, Gretz N. miRWalk–database: prediction of possible miRNA binding sites by "walking" the genes of three genomes. J Biomed Inform 2011; 44: 839–47.

European Chromosome 16 Tuberous Sclerosis Consortium. Identification and characterization of the tuberous sclerosis gene on chromosome 16. Cell 1993; 75: 1305–15.

Fabregat A, Jupe S, Matthews L, Sidiropoulos K, Gillespie M, Garapati P, et al. The reactome pathway knowledgebase. Nucleic Acids Res 2018; 46: D649–55.

Filipek PA, de Araujo MEG, Vogel GF, De Smet CH, Eberharter D, Rebsamen M, et al. LAMTOR/Ragulator is a negative regulator of Arl8b- and BORC-dependent late endosomal positioning. J Cell Biol 2017; 216: 4199–215.

Franz DN, Agricola K, Mays M, Tudor C, Care MM, Holland-Bouley K, et al. Everolimus for subependymal giant cell astrocytoma: 5-year final analysis. Ann Neurol 2015; 78: 929–38.

Franz DN, Belousova E, Sparagana S, Bebin EM, Frost M, Kuperman R, et al. Everolimus for subependymal giant cell astrocytoma in patients with tuberous sclerosis complex: 2-year open-label extension of the randomised EXIST-1 study. Lancet Oncol 2014; 15: 1513–20.

Franz DN, Belousova E, Sparagana S, Bebin EM, Frost M, Kuperman R, et al. Efficacy and safety of everolimus for subependymal giant cell astrocytomas associated with tuberous sclerosis complex (EXIST-1): a multicentre, randomised, placebo-controlled phase 3 trial. Lancet 2013; 381: 125–32.

Franz DN, Leonard J, Tudor C, Chuck G, Care M, Sethuraman G, et al. Rapamycin causes regression of astrocytomas in tuberous sclerosis complex. Ann Neurol 2006; 59: 490–8.

Fujiwara S, Takaki T, Hikita T, Nishio S. Subependymal giant-cell astrocytoma associated with tuberous sclerosis. Do subependymal nodules grow? Childs Nerv Syst 1989; 5: 43–4.

Glazova MV, Nikitina LS, Hudik KA, Kirillova OD, Dorofeeva NA, Korotkov AA, et al. Inhibition of ERK1/2 signaling prevents epileptiform behavior in rats prone to audiogenic seizures. J Neurochem 2015; 132: 218–29.

Goh S, Butler W, Thiele EA. Subependymal giant cell tumors in tuberous sclerosis complex. Neurology 2004; 63: 1457–61.

Gorter JA, Iyer A, White I, Colzi A, van Vliet EA, Sisodiya S, et al. Hippocampal subregion-specific microRNA expression during epileptogenesis in experimental temporal lobe epilepsy. Neurobiol Dis 2014; 62: 508–20.

Govindarajan B, Mizesko MC, Miller MS, Onda H, Nunnelley M, Casper K, et al. Tuberous sclerosis-associated neoplasms express activated p42/44 mitogen-activated protein (MAP) kinase, and inhibition of MAP kinase signaling results in decreased in vivo tumor growth. Clin Cancer Res 2003; 9: 3469–75.

Griffiths-Jones S, Saini HK, van Dongen S, Enright AJ. miRBase: tools for microRNA genomics. Nucleic Acids Res 2008; 36: D154–8.

Han S, Santos TM, Puga A, Roy J, Thiele EA, McCollin M, et al. Phosphorylation of tuberin as a novel mechanism for somatic inactivation of the tuberous sclerosis complex proteins in brain lesions. Cancer Res 2004; 64: 812–6.

Harrow J, Frankish A, Gonzalez JM, Tapanari E, Diekhans M, Kokocinski F, et al. GENCODE: the reference human genome annotation for The ENCODE Project. Genome Res 2012; 22: 1760–74.

Huang da W, Sherman BT, Lempicki RA. Bioinformatics enrichment tools: paths toward the comprehensive functional analysis of large gene lists. Nucleic Acids Res 2009a; 37: 1–13.

Huang da W, Sherman BT, Lempicki RA. Systematic and integrative analysis of large gene lists using DAVID bioinformatics resources. Nat Protoc 2009b; 4: 44–57.

Inoki K, Li Y, Xu T, Guan KL. Rheb GTPase is a direct target of TSC2 GAP activity and regulates mTOR signaling. Genes Dev 2003; 17: 1829–34.

Jozwiak S, Mandera M, Mlynarski W. Natural history and current treatment options for subependymal giant cell astrocytoma in tuberous sclerosis complex. Semin Pediatr Neurol 2015; 22: 274–81.

Kim D, Pertea G, Trapnell C, Pimentel H, Kelley R, Salzberg SL. TopHat2: accurate alignment of transcriptomes in the presence of insertions, deletions and gene fusions. Genome Biol 2013; 14: R36.

Kingswood JC, d'Augeres GB, Belousova E, Ferreira JC, Carter T, Castellana R, et al. TuberOus SClerosis registry to increase disease awareness (TOSCA)-baseline data on 2093 patients. Orphanet J Rare Dis 2017; 12: 2.

Korotkov A, Broekaart DWM, van Scheppingen J, Anink JJ, Baayen JC, Idema S, et al. Increased expression of matrix metalloproteinase 3 can be attenuated by inhibition of microRNA-155 in cultured human astrocytes. J Neuroinflamm 2018; 15: 211.

Kothare SV, Singh K, Chalifoux JR, Staley BA, Weiner HL, Menzer K, et al. Severity of manifestations in tuberous sclerosis complex in relation to genotype. Epilepsia 2014; 55: 1025–9.

Kotulska K, Borkowska J, Roszkowski M, Mandera M, Daszkiewicz P, Drabik K, et al. Surgical treatment of subependymal giant cell astrocytoma in tuberous sclerosis complex patients. Pediatr Neurol 2014; 50: 307–12.

Kotulska K, Chmielewski D, Borkowska J, Jurkiewicz E, Kuczynski D, Kmiec T, et al. Long-term effect of everolimus on epilepsy and growth in children under 3 years of age treated for subependymal giant cell astrocytoma associated with tuberous sclerosis complex. Eur J Paediatr Neurol 2013; 17: 479–85.

Krueger DA, Care MM, Agricola K, Tudor C, Mays M, Franz DN. Everolimus long-term safety and efficacy in subependymal giant cell astrocytoma. Neurology 2013; 80: 574–80.

Krueger DA, Care MM, Holland K, Agricola K, Tudor C, Mangeshkar P, et al. Everolimus for subependymal giant-cell astrocytomas in tuberous sclerosis. N Engl J Med 2010; 363: 1801–11.

Krueger DA, Wilfong AA, Mays M, Talley CM, Agricola K, Tudor C, et al. Long-term treatment of epilepsy with everolimus in tuberous sclerosis. Neurology 2016; 87: 2408–15.

Liao Y, Smyth GK, Shi W. featureCounts: an efficient general purpose program for assigning sequence reads to genomic features. Bioinformatics 2014; 30: 923–30.

Louis DN, Perry A, Reifenberger G, von Deimling A, Figarella-Branger D, Cavenee WK, et al. The 2016 World Health Organization classification of tumors of the central nervous system: a summary. Acta Neuropathol 2016; 131: 803–20.

Love MI, Huber W, Anders S. Moderated estimation of fold change and dispersion for RNA-seq data with DESeq2. Genome Biol 2014; 15: 550.

Ma L, Chen Z, Erdjument-Bromage H, Tempst P, Pandolfi PP. Phosphorylation and functional inactivation of TSC2 by Erk implications for tuberous sclerosis and cancer pathogenesis. Cell 2005; 121: 179–93.

Ma L, Teruya-Feldstein J, Bonner P, Bernardi R, Franz DN, Witte D, et al. Identification of S664 TSC2 phosphorylation as a marker for extracellular signal-regulated kinase mediated mTOR activation in tuberous sclerosis and human cancer. Cancer Res 2007; 67: 7106–12.

Martin KR, Zhou W, Bowman MJ, Shih J, Au KS, Dittenhafer-Reed KE, et al. The genomic landscape of tuberous sclerosis complex. Nat Commun 2017; 8: 15816.

Martins F, de Oliveira MA, Wang Q, Sonis S, Gallottini M, George S, et al. A review of oral toxicity associated with mTOR inhibitor therapy in cancer patients. Oral Oncol 2013; 49: 293–8.

McCormack FX, Inoue Y, Moss J, Singer LG, Strange C, Nakata K, et al. Efficacy and safety of sirolimus in lymphangioleiomyomatosis. N Engl J Med 2011; 364: 1595–606.

Mi R, Ma J, Zhang D, Li L, Zhang H. Efficacy of combined inhibition of mTOR and ERK/MAPK pathways in treating a tuberous sclerosis complex cell model. J Genet Genomics 2009; 36: 355–61.

Mills JD, Iyer AM, van Scheppingen J, Bongaarts A, Anink JJ, Janssen B, et al. Coding and small non-coding transcriptional landscape of tuberous sclerosis complex cortical tubers: implications for pathophysiology and treatment. Sci Rep 2017; 7: 8089.

Mizuguchi M, Takashima S. Neuropathology of tuberous sclerosis. Brain Dev 2001; 23: 508–15.

Morimoto K, Mogami H. Sequential CT study of subependymal giant-cell astrocytoma associated with tuberous sclerosis. Case report. J Neurosurg 1986; 65: 874–7.

Nabbout R, Santos M, Rolland Y, Delalande O, Dulac O, Chiron C. Early diagnosis of subependymal giant cell astrocytoma in children with tuberous sclerosis. J Neurol Neurosurg Psychiatry 1999; 66: 370–5.

Nada S, Mori S, Takahashi Y, Okada M. p18/LAMTOR1: a late endosome/lysosome-specific anchor protein for the mTORC1/MAPK signaling pathway. Methods Enzymol 2014; 535: 249–63.

Nateri AS, Raivich G, Gebhardt C, Da Costa C, Naumann H, Vreugdenhil M, et al. ERK activation causes epilepsy by stimulating NMDA receptor activity. EMBO J 2007; 26: 4891–901.

Northrup H, Krueger DA, International Tuberous Sclerosis Complex Consensus G. Tuberous sclerosis complex diagnostic criteria update: recommendations of the 2012 International Tuberous Sclerosis Complex Consensus Conference. Pediatr Neurol 2013; 49: 243–54.

Pernice HF, Schieweck R, Kiebler MA, Popper B. mTOR and MAPK: from localized translation control to epilepsy. BMC Neurosci 2016; 17: 73.

Prabowo AS, Anink JJ, Lammens M, Nellist M, van den Ouweland AM, Adle-Biassette H, et al. Fetal brain lesions in tuberous sclerosis complex: TORC1 activation and inflammation. Brain Pathol 2013; 23: 45–59.

Ramakers C, Ruijter JM, Deprez RH, Moorman AF. Assumption-free analysis of quantitative real-time polymerase chain reaction (PCR) data. Neurosci Lett 2003; 339: 62–6.

Rebsamen M, Pochini L, Stasyk T, de Araujo ME, Galluccio M, Kandasamy RK, et al. SLC38A9 is a component of the lysosomal amino acid sensing machinery that controls mTORC1. Nature 2015; 519: 477–81.

Ruijter JM, Ramakers C, Hoogaars WM, Karlen Y, Bakker O, van den Hoff MJ, et al. Amplification efficiency: linking baseline and bias in the analysis of quantitative PCR data. Nucleic Acids Res 2009; 37: e45.

Sadowski K, Kotulska K, Jozwiak S. Management of side effects of mTOR inhibitors in tuberous sclerosis patients. Pharmacol Rep 2016; 68: 536–42.

Sancak Y, Bar-Peled L, Zoncu R, Markhard AL, Nada S, Sabatini DM. Ragulator-Rag complex targets mTORC1 to the lysosomal surface and is necessary for its activation by amino acids. Cell 2010; 141: 290–303.

Sancak Y, Peterson TR, Shaul YD, Lindquist RA, Thoreen CC, Bar-Peled L, et al. The Rag GTPases bind raptor and mediate amino acid signaling to mTORC1. Science 2008; 320: 1496–501.

Shannon P, Markiel A, Ozier O, Baliga NS, Wang JT, Ramage D, et al. Cytoscape: a software environment for integrated models of biomolecular interaction networks. Genome Res 2003; 13: 2498–504.

Shao Y, Wang C, Hong Z, Chen Y. Inhibition of p38 mitogen-activated protein kinase signaling reduces multidrug transporter activity and anti-epileptic drug resistance in refractory epileptic rats. J Neurochem 2016; 136: 1096–105.

Smedley D, Haider S, Ballester B, Holland R, London D, Thorisson G, et al. BioMart–biological queries made easy. BMC Genomics 2009; 10: 22.

Teis D, Wunderlich W, Huber LA. Localization of the MP1-MAPK scaffold complex to endosomes is mediated by p14 and required for signal transduction. Dev Cell 2002; 3: 803–14.

Trapnell C, Roberts A, Goff L, Pertea G, Kim D, Kelley DR, et al. Differential gene and transcript expression analysis of RNA-seq experiments with TopHat and Cufflinks. Nat Protoc 2012; 7: 562–78.

Tyburczy ME, Kotulska K, Pokarowski P, Mieczkowski J, Kucharska J, Grajkowska W, et al. Novel proteins regulated by mTOR in subependymal giant cell astrocytomas of patients with tuberous sclerosis complex and new therapeutic implications. Am J Pathol 2010; 176: 1878–90.

van Scheppingen J, Iyer AM, Prabowo AS, Muhlebner A, Anink JJ, Scholl T, et al. Expression of microRNAs miR21, miR146a, and miR155 in tuberous sclerosis complex cortical tubers and their regulation in human astrocytes and SEGA-derived cell cultures. Glia 2016; 64: 1066–82.

van Scheppingen J, Mills JD, Zimmer TS, Broekaart DWM, Iori V, Bongaarts A, et al. miR147b: A novel key regulator of interleukin 1 beta-mediated inflammation in human astrocytes. Glia 2018; 66: 1082–97.

van Slegtenhorst M, de Hoogt R, Hermans C, Nellist M, Janssen B, Verhoef S, et al. Identification of the tuberous sclerosis gene TSC1 on chromosome 9q34. Science 1997; 277: 805–8.

Varemo L, Nielsen J, Nookaew I. Enriching the gene set analysis of genome-wide data by incorporating directionality of gene expression and combining statistical hypotheses and methods. Nucleic Acids Res 2013; 41: 4378–91.

Wang S, Tsun ZY, Wolfson RL, Shen K, Wyant GA, Plovanich ME, et al. Metabolism. Lysosomal amino acid transporter SLC38A9 signals arginine sufficiency to mTORC1. Science 2015; 347: 188–94.

Wunderlich W, Fialka I, Teis D, Alpi A, Pfeifer A, Parton RG, et al. A novel 14-kilodalton protein interacts with the mitogen-activated protein kinase scaffold mp1 on a late endosomal/lysosomal compartment. J Cell Biol 2001; 152: 765–76.

Zhang B, Zou J, Rensing NR, Yang M, Wong M. Inflammatory mechanisms contribute to the neurological manifestations of tuberous sclerosis complex. Neurobiol Dis 2015; 80: 70–9.

Zurolo E, Iyer A, Maroso M, Carbonell C, Anink JJ, Ravizza T, et al. Activation of toll-like receptor, RAGE and HMGB1 signalling in malformations of cortical development. Brain 2011; 134: 1015–32.